Anomalous composition-dependent dynamics of nanoconfined water in the interlayer of disordered calcium-silicates

Mohammad Javad Abdolhosseini Qomi, Mathieu Bauchy,[a] Franz-Josef Ulm,[a] and Roland J.-M. Pellenq[b]
Concrete Sustainability Hub, Department of Civil and Environmental Engineering, Massachusetts Institute of Technology, 77 Massachusetts Avenue, Cambridge, Massachusetts 02139, USA

(Received 13 December 2013; accepted 22 January 2014; published online 7 February 2014)

With shear interest in nanoporous materials, the ultraconfining interlayer spacing of calcium–silicate–hydrate (C–S–H) provides an excellent medium to study reactivity, structure, and dynamic properties of water. In this paper, we present how substrate composition affects chemo-physical properties of water in ultraconfined hydrophilic media. This is achieved by performing molecular dynamics simulation on a set of 150 realistic models with different compositions of calcium and silicon contents. It is demonstrated that the substrate chemistry directly affects the structural properties of water molecules. The motion of confined water shows a multi-stage dynamics which is characteristic of supercooled liquids and glassy phases. Inhomogeneity in that dynamics is used to differentiate between mobile and immobile water molecules. Furthermore, it is shown that the mobility of water molecules is composition-dependent. Similar to the pressure-driven self-diffusivity anomaly observed in bulk water, we report the first study on composition-driven diffusion anomaly, the self diffusivity increases with increasing confined water density in C–S–H. Such anomalous behavior is explained by the decrease in the typical activation energy required for a water molecule to escape its dynamical cage. © *2014 AIP Publishing LLC*. [http://dx.doi.org/10.1063/1.4864118]

I. INTRODUCTION

The advancements in the synthesis of nanoporous materials have led to the development of efficient water desalination systems,[1] catalyst-containing nanocapsules,[2] organic-based zeolitic-like frameworks,[3,4] and porous carbon[5] for hydrogen storage. Efficiency of these nanomaterials is closely tied to the state of water and cations within the nanoconfinements and their exchange through the mesoporous surfaces.[6] In addition, the three water molecules – thick interfacial water – within biological cells has shown to influence a wide range of attributes in the frame of non-adaptive genomic level.[7,8] The confinement size and pore geometry directly affect the chemo-physical properties of water, such as shift in dipole moment,[9] hydrogen bonding,[10] and transport properties;[11] these are significantly different from those of bulk water. Despite the multi-disciplinary interests in understanding water in confined geometries, our knowledge on the field of interfacial properties of water in such extreme confining conditions is still in a fledgling state.

The nano-texture of calcium–silicate–hydrate (C–S–H) and the binding phase in cement paste is responsible for its strength, durability, and creep properties.[12] This hydration product is a versatile medium, which is used to study chemo-physical properties of confined water. Despite its ubiquitous presence in the built environment, the layered C–S–H structure at an atomistic level has only been recently discovered.[13,14] With growing evidences on the nanogranular texture of C–S–H,[15–18] the C–S–H particles appear to be excellent analogs of nanocapsules with porous surfaces that enable inter-particle water and cationic exchange. However, the difference between the interlayer and inter-particle pore size distributions results in a broad distribution of residence times of water molecules. This leads to partial decomposition and averaged representation of dynamical quantities in Neutron Scattering (NS)[19] and Proton Field-Cycling Relaxometry (PFCR)[20] experiments. This highlights the relevance of atomistic simulation techniques that provide insights into experimentally inaccessible measurements. In fact, these experimentally aggregated descriptions are at the origin of classifying water into free, constrained, and chemically bounded water molecules using the Quasi-Elastic Neutron Scattering method.[21] Consequently, this has led to classifying the dynamical properties of confined water as "glass-like" behavior, reminiscent of characteristics of supercooled liquids and glassy phases.[22–25] Yet, the effects of confinement stoichiometry by modification of surface chemistry and morphology on properties of confined water remain to be investigated.

The main focus of this paper is to understand how chemical modification of C–S–H influences the structural and dynamical properties of water. In fact, we attempt to answer long-standing questions about the mobility of water in ultraconfined hydrophilic interlaminar spacing and its comparison with inter-particle and bulk water. This paper has been organized into four different sections. Section II covers the details

[a] Also at $\langle MSE \rangle^2$, MIT-CNRS Joint Laboratory at Massachusetts Institute of Technology, 77 Massachusetts Avenue, Cambridge, Massachusetts 02139, USA.
[b] Electronic mail: pellenq@mit.edu. Also at $\langle MSE \rangle^2$, MIT-CNRS Joint Laboratory at Massachusetts Institute of Technology, 77 Massachusetts Avenue, Cambridge, Massachusetts 02139, USA and Centre Interdisciplinaire de Nanosciences de Marseille, CNRS and Aix-Marseille Universite, Campus de Luminy, 13288 Marseille Cedex 09, France.

of molecular dynamics simulation and molecular structure of C–S–H at different stoichiometries. Section III is divided into five subsections. First subsection discusses the effect of stoichiometry on the structure of water such as bond length, dipolar moment, density, or hydrogen bond network. Consecutive three subsections delve into anisotropy and inhomogeneity of water dynamics in a confined medium. Finally, the last subsection presents the effect of confinement chemistry on the self-diffusivity and identifies a new anomalous behavior of water under extreme confinement. Section IV draws final conclusions and summarizes our findings.

II. METHODS

A. Molecular models and force fields

To describe the disordered molecular structure of C–S–H, Pellenq *et al.*[28] proposed a realistic model for C–S–H with the stoichiometry of $(CaO)_{1.65}(SiO_2)(H_2O)_{1.73}$. In this work, a set of 150 realistic molecular structures for C–S–H is constructed with varying Ca/Si ratios ranging from 1.1 to 2.1. Following a combinatorial procedure, the C–S–H models are constructed by chemically and structurally modifying 11 Å tobermorite.[29] 11 Å tobermorite consists of pseudo-octahedral calcium oxide sheets sandwiched by dreierketten silica tetrahedral chains. Silicate chains only consist of pairing (bridging oxygen atoms) and bridging sites (having two bridging and two dangling oxygen atoms).[30] These negatively charged calcium-silicate sheets are separated from each other by interlayer spacing, which incorporate "interlayer" water molecules and charge-balancing calcium cations ($4.8\ \frac{\bar{e}}{nm^2}$). While the Ca/Si ratio in 11 Å tobermorite is 1, this ratio is systematically increased in C–S–H models through randomly removing SiO_2 groups. Defects in silicate chains provide possible sites for adsorption of extra water molecules. Adsorption of water molecules in the structurally defected tobermorite models was performed via the Grand Canonical Monte-Carlo (GCMC) method ensuring equilibrium with bulk water at constant volume and room temperature and is denoted as "adsorbed water" in Fig. 1. The simulated number of hydrogen atoms in water molecules and hydroxyl groups per silicon atom (H/Si) is in full agreement with drying[27] and Small Angle Neutron Scattering (SANS)[15] experiments.

As shown in Fig. 1, these models provide molecular structures of C–S–H that are consistent with the experimental stoichiometry of $(CaO)_x(SiO_2)(H_2O)_{2(x-1)+0.5+\delta}$ where δ is associated with the polymorphic structure of C–S–H providing a variation of water content based on the combinatorial nature of silicate arrangements at the nano-scale. Some of the above-mentioned interlayer water molecules are chemically unstable and dissociated into hydroxyl groups and protons upon first principle or reactive force field modeling. In this work, we use REAXFF potential[26] to enforce the reaction between the interlayer water and the defective calcium-silicate sheets.[31] Unreacted water molecules are denoted in Fig. 1 as "structural water." The reactive modeling further refines the stoichiometry by adding an extra dimension: $(CaO)_x(SiO_2)(H_2O)^{\text{Unreacted}}_{1.2(x-1)+0.3+\beta}(H_2O)^{\text{Hydroxylating}}_{0.8(x-1)+0.2+\gamma}$ where extra parameters β and γ introduce the effect of polymorphism to the stoichiometry. It should be emphasized that "Unreacted" and "Hydroxylating" superscripts indicate, respectively, unreacted and dissociated water molecules during reactive simulations. Furthermore, both drying and SANS experiments measure the total hydrogen content and cannot distinguish between hydrogen atoms in molecular water or hydroxyl groups. The collective topological observation of these 150 numerical samples indicates that, while C–S–H below Ca/Si ratio of 1.5 has a crystalline molecular structure, it has a local glassy structure at high Ca/Si ratios above 1.5, while still retaining some long-range layered texture.

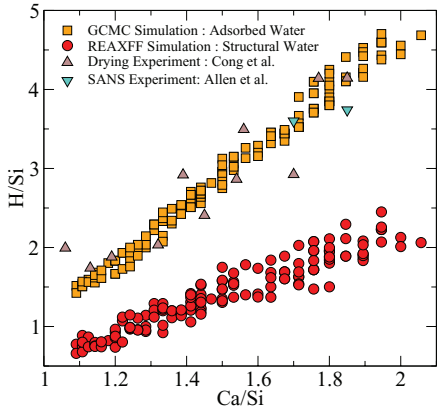

FIG. 1. State of hydrogen in C–S–H nanotexture as a function of stoichiometry. The total hydrogen content calculated via a combination of grand canonical Monte Carlo and molecular dynamics simulations based on REAXFF potential[26] compared to drying experiment of Cong and Kirkpatrick[27] and Small Angle Neutron Scattering (SANS) experiment of Allen *et al.*[15]

In this work, equilibrium molecular dynamics (MD) simulations are performed on the reacted C–S–H samples with the focus on understanding the structure and mobility of unreacted interlayer water molecules. Several studies have suggested the importance of incorporating flexibility in modeling confined water in hydrophobic and hydrophilic confinements and ionic solutions.[11,32,33] To resolve the issues related to incorporating rigid water models such as SPC/E, a flexible but unpolarizable version of SPC model, which reproduces the structure and properties of water at ambient temperature, was employed.[34,35] Core-only potential CSH-FF,[36] which is a clayff-like potential,[37] is used in our calculations, as it reproduces the structure and mechanics of C–S–H at various stoichiometry which has been shown to be in good agreement with density functional theory (DFT) calculations on crystalline C–S–H such as tobermorite polymorphs.[36] To avoid the expenses incurred by calculating coulombic interactions in real and reciprocal spaces, such interactions are calculated via the Wolf method.[38] In the supplementary material further details on the preparation of C–S–H structures and the force fields are provided.[39]

B. Molecular dynamics

In this work, all MD trajectories for 150 C–S–H models were produced using LAMMPS.[40] The equations of motion were integrated via the Velocity-Verlet algorithm. The

time steps are set as small as 1 fs to reproduce the dynamics of O–H bonds. All 150 samples were relaxed in isobaric-isothermal ensemble (NPT) with the target temperature of 300 K and pressure of 0 atm. To reproduce the dynamics of water at different time-scales, all simulations were taken to the microcanonical ensemble (NVE) to start two separate sets of simulations for the production phase. This choice was made to avoid the usage of any thermostat that could affect the dynamics of water. We ensured that the temperature remained constant throughout the simulation. The first set of simulations, intended to describe the dynamics at short time scales, was 100 ps long with configurations saved every 100 fs. The second set of simulations was 10 ns long with outputs recorded on intervals of 10 ps. The selection of time intervals was based on Churakov prediction that 10 ns long simulations are necessary to capture the diffusion of water in the interlayer of tobermorite minerals.[41] To compare the effect of confinement on water molecules with that of bulk, a box of water with 1200 water molecules was simulated and hereafter referred as being either "bulk" or "SPC" water. To calculate the structural and dynamical properties of interlayer water, several post-processing scripts were written to analyze the trajectories.

III. RESULTS AND DISCUSSIONS

This section is divided into five subsections. First, the effects of C–S–Hs composition on the short-range structural characteristics of confined water are presented in detail. These analyses include O–H bond stretch factor, Voronoi analysis of accessible volume, and average number of hydrogen bonding per water molecule. Second, the mean square displacement is examined to reveal the dynamics of interlayer water. The third subsection is dedicated to the Van Hove space-time correlation function to investigate the inhomogeneous nature of water mobility in C–S–H molecular structure. In the fourth part, the inhomogeneity analysis is extended to a wide range of chemistries and the probabilistic picture of water mobility is portrayed in function of the Ca/Si ratio. Finally, the fifth subsection analyzes the quasi two-dimensional self-diffusivity of mobile water and its anomalous correlation with density in the C–S–H interlamellar spacing.

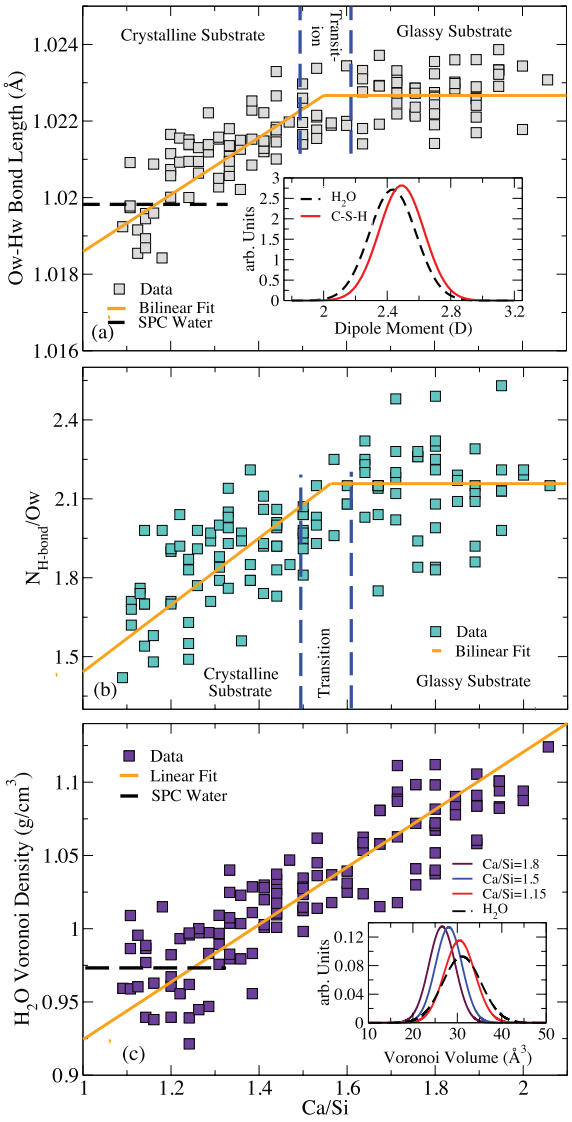

FIG. 2. Effect of substrate stoichiometry on the characteristics of confined water. (a) Ow–Hw bond length as a function of Ca/Si ratio. The inset shows the distribution of dipole moments in C–S–H (Ca/Si = 1.75) against bulk water. The stretch of Ow–Hw results in the increase in dipole moment of water in confined medium. Ow and Hw denote oxygen and hydrogen in water molecules, respectively. (b) The effect of Ca/Si ratio on the number of hydrogen bonds per water molecule. (b) Effect of Ca/Si ratio on the Voronoi density of interlayer water compared to that of bulk SPC water. The inset displays the distribution of Voronoi volume of water molecules for C–S–Hs of varying compositions against that of SPC bulk water.

A. Structure of confined water

By closely looking at water density profiles in the vicinity of calcium-silicate sheets, Youssef *et al.*[22] found excess water concentration at the surfaces. Also, it was realized that hydrogen atoms of water have a tendency of moving toward the surface. These are clear signs of hydrophilicity of calcium-silicate sheets that directly affect the structure of water.

Figure 2 presents the effect of the stoichiometry of C–S–H on the structure of water in the interlayer spacing. The structure of water is directly affected by the availability of adsorption sites on the calcium-silicate surfaces. Figure 2(a) presents the effect of stoichiometry on the equilibrium O–H bond length. The O–H bond length in C–S–H microporous medium is larger than that of bulk water. This means that the interaction between C–S–H hydrophilic surfaces and protons in water molecules stretches the bond length. The O–H bond length in SPC water increases linearly from 1.018 Å to 1.022 Å in the crystalline substrate domain and reaches a plateau in the glassy domain. The physical reason behind the plateau response in high Ca/Si ratio is that the extra water is less affected by the surface through a shielding mechanism. In fact, adsorbed water molecules, adjacent to the surface, screen electrostatic interactions between the additional water molecules and non-bridging oxygen atoms.[42] While the O–H bond length is directly influenced by the hydrophilicity of C–S–H substrate, the H-O-H angular distribution does not show any significant statistical differences. This directly affects the

dipole moment of water molecules in the interlayer spacing. Inset in Figure 2(a) provides the distribution of the dipole moment in the Ca/Si = 1.75 C–S–H sample compared to that of bulk water. Statistically, the dipole moment of confined water, 2.56 ± 0.3 D, follows normal distribution with first moment higher than that of bulk water, 2.50 ± 0.3 D. In contrast to hydrophobic zeolite micropores,[9,43] the upshift of dipole moment is the signature of the hydrophilicity of C–S–H surfaces. The hydrophilicity of nanopores, not only affects the internal structure of water molecules but also the way water molecules are packed in the interlayer spacing. This packing affects the accessible volume and the density of water in ultra-confined environment.

Higher packing and proper orientation of water molecules increase the probability of forming hydrogen bonds network. There are numerous ways to identify hydrogen bonds based on either energetic[44,45] or geometrical criteria.[46] Following the method of Luzar and Chandler,[47,48] the hydrogen bonds are solely distinguished by geometrical rules satisfying $d_{O-O} < 3.5$ Å and $\theta_{H-O-O} < 30^{\circ}$, where d_{O-O} is the distance between the hydrogen donor and acceptor oxygen atoms and θ_{H-O-O} is the angle between O–H ray in the donor and O–O ray connecting oxygen in the donor and the acceptor. Figure 2(b) displays the effect of C–S–H's substrate stoichiometry on the number of H-bonds per water molecule. Similar to glycerol/water mixtures[49] and water in clay nanoscale galleries,[50] the number of H-bonds is significantly lower than that of bulk water, approximately 3.6 H-bond per water molecules. The number of H-bonds increases linearly in the crystalline domain from 1.5 to 2.15 H-bonds per water molecule and maintains a constant value in the glassy domain. Using the potential-of-mean-force approach (PMF), Youssef *et al.*[22] calculated the value of 2.3 H-bonds per water molecule for Ca/Si = 1.7 which is in close agreement with these results. The increase in the number of hydrogen bonds with Ca/Si ratio is in agreement with the infrared spectroscopy experiment of Yu *et al.*[51] They explained the broadening of the peak corresponding to Ow–Hw stretch mode by the increase in the number of hydrogen bonds.

The packing of water molecules in the interlayer spacing affects the density of C–S–H particles.[52] This necessitates a fresh look on the definition of density of water in confined geometries. This is achieved by employing topological geometry approaches in the context of nano-scale confinements. The Voronoi tessellation algorithm is one of the commonly used methods. To exemplify, it was applied to the structural analysis of liquid glass formers,[53] liquid-gas interfaces,[54] and ice nucleation.[55] In periodic systems, Voronoi volume is a portion of the space around a particle in which every point is closer to that particle than any other particle. The Voronoi density can be defined as the mass of particles divided by their Voronoi volume. In the case of bulk water, the conventional and Voronoi densities are identical. However, the ultra-confined medium in the interlayer spacing affects the Voronoi volume of water molecule and, hence, their Voronoi density. Figure 2(c) provides the relation between the stoichiometry of C–S–H and Voronoi density of water in the interlayer spacing. The water density increases linearly with the Ca/Si ratio. The adsorption of roughly 1.2 structural water molecules caused by removal of SiO_2 group asserts that the density of interlayer water is controlled by the availability of adsorption sites to a higher extent. At low Ca/Si ratios, the density of water is close to that of SPC bulk water. However, at high Ca/Si ratios, the density of water is around 1.12 g/cm^3, which is significantly larger than that of bulk water. This is explained more thoroughly in the inset of the Figure 2(c). This figure exhibits the Voronoi volume distribution for bulk water against three different chemical compositions. All distributions, either bulk or confined, follow normal distribution. At low Ca/Si ratios, Ca/Si = 1.15, the first moment of volume distribution for confined and bulk water is identical. However, the second moment is smaller in the case of confined water, which means that the motion of water molecules is very limited in C–S–H interlayer space. At high Ca/Si ratios, Ca/Si = 1.5 and 1.8, both the first and second moment of volume distribution are smaller than that of the bulk. The ultra-packing of water molecules in C–S–H is similar to that of the hydration shell of proteins.[56,57] Now that we have demonstrated the effects of chemistry on the structure of water, it is important to investigate the mobility of water in the C–S–H interlayer space.

B. Inhomogeneity and anisotropy in water dynamics

Due to the strong hydrophilicity of calcium-silicate layers, the width and roughness of interlayer voids, the dynamics of water in the interlayer spacing of C–S–H is expected to be heterogeneous. This can be characterized by the mean square displacement (MSD) and the self part of the Van Hove space-time correlation function. By utilizing the principle of invariance under time translation in equilibrium, the MSD of an atom is defined as

$$\mathrm{MSD}_i(t) = \Delta r_i^2(t) = \langle |r_i(t+\tau) - r_i(\tau)|^2 \rangle, \qquad (1)$$

where r_i denotes the coordinates of oxygen atom i in water and the bracket represents time averaging at multiple time origins, τ. To illustrate the dynamical inhomogeneity of water, the MSDs of individual water molecules across all 150 samples were studied extensively. To illustrate, Figure 3 presents individual MSDs of water molecules within the range of 100 to 10 000 ps in a sample with Ca/Si ratio of 1.4. The set of those individual MSDs clearly proves the validity of the aforementioned hypothesis on dynamical inhomogeneity. That is, water molecules can be divided into two categories: mobile and immobile. Immobile water molecules have limited motion around their adsorption sites, which is characteristic of librational dynamics in an ultraconfining cage around interlayer calcium or in the vicinity of defective silica chains. On the contrary, mobile water exhibits less bounded motion in the interlayer spacing, which resembles to diffusive dynamics in supercooled liquids. The distinction between mobile and immobile water molecules is based on two arguments. First of all, the root mean square displacements (RMSDs) of immobile and mobile water are significantly different. While the final RMSD of immobile water is smaller than 2 Å, the RMSD of mobile water is larger. The 2 Å length scale is referred to as the typical cage radius and hence is denoted by d_{cage}. Second, the slope of MSD in mobile and immobile water is clearly

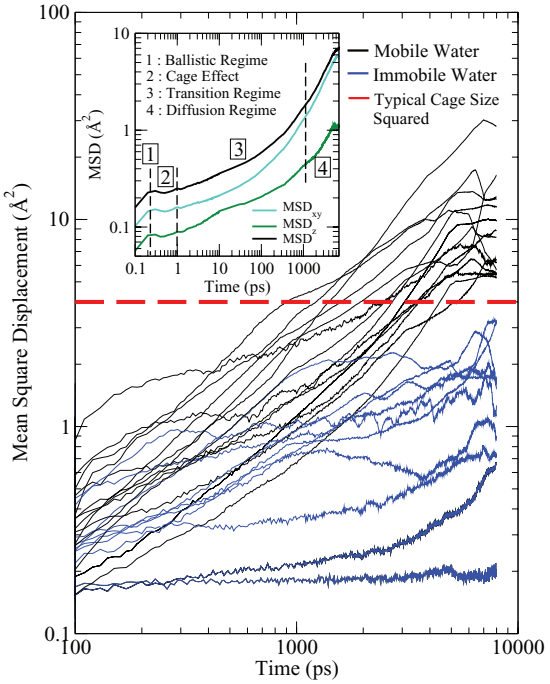

FIG. 3. Mean square displacement (MSD) as a function of time for each water molecule in a sample with Ca/Si = 1.4. The inset presents the total average MSD and average MSD parallel and perpendicular to the calcium-silicate layers. The dashed red line at 4 Å^2 is used to define the cage size, d_{cage} (see text).

different. While the slope of MSD versus time in mobile water is larger than zero, the slope of MSD of immobile water is close to 0 (at time scales lower than 1 ns). This inhomogeneity in mobility is also observed in supercooled bulk water[58] and clay-zeolite composites.[59]

The inset of Figure 3 displays the average MSD in the range of 0.1 ps to 10 ns. It demonstrates the dynamically slow nature of confined water in C–S–H, which can be partitioned in four stages, analogous to that of dense fluids and supercooled phases.[60] The four stages are ballistic, cage, transition, and diffusion regimes. At very short times, t $\leq$ 200 fs, the water molecules move just ballistically,[61] $\langle r^2(t)\rangle \propto t^2$. In the second stage, within intermediate time scales, MSD follows a plateau up to 1 ps. This is mainly because water molecules rattle around in the cage formed by neighboring particles colliding with water molecules and calcium layer species. Subsequently, parts of water molecules succeed to escape the cage, which can be associated with the intermediate stage. The motion of water molecules in the transition regime can be described as diffusion with low exponent ($\langle r^2(t)\rangle \propto t^\alpha$ where $\alpha < 1$). The transition with exponent smaller than one is also observed in supercooled liquids and attributed to inhomogeneous non-Gaussian collective hopping of particles.[62] The diffusion exponent gradually increases in the third stage until it reaches that of a diffusion regime, $\langle r^2(t)\rangle \propto t$.

Due to the small width to length ratio of interlayer channels ($\approx\frac{1}{10}$), the diffusion inside C–S–H particles has characteristics of a quasi two-dimensional diffusion. This anisotropy in the diffusion can be quantified via the components of average MSD:[63]

$$MSD_{xy} = \frac{1}{N}\sum_{i=1}^{N}\Delta x_i^2(t) + \Delta y_i^2(t), \tag{2}$$

$$MSD_z = \frac{1}{N}\sum_{i=1}^{N}\Delta z_i^2(t), \tag{3}$$

where N is the number of water molecules, MSD_{xy} and MSD_z denote the parallel and perpendicular parts of the MSD. As it is shown in the inset of Figure 3, the MSD_{xy} is almost one order of magnitude larger than MSD_z. This emphasizes that the diffusion is strongly controlled by the interlayer space width presenting nearly two-dimensional characteristics.[42,64,65]

C. Inhomogeneity characterization via the Van Hove correlation function

To further characterize the inhomogeneous dynamics of water, the self part of Van Hove space-time correlation function is employed.[66] This function is defined as

$$G_s(r,t) = \frac{1}{N}\sum_{i=1}^{N}\langle\delta(r - |r_i(t+\tau) - r_i(\tau)|)\rangle, \tag{4}$$

where δ denotes the Kronecker function. This correlation function allows us to determine the probability[67] $2\pi r G_s(r,t)$ that a water molecule originally at ($t = 0$) and ($r = 0$) has moved by a distance r after elapsing time t. Following the discussion on the anisotropy of diffusion in the C–S–H, the planar $2\pi r$ factor is adopted instead of the usual $4\pi r^2$ in three-dimensional diffusion, as the motion of mobile water molecules is characterized by quasi two-dimensional diffusion. Presenting the results only for a sample with Ca/Si = 1.4, Figure 4(a) provides the Van Hove correlation function at different time scales. At short time-scales, ($t \approx$ 1ps), water molecules are still in the cage. At longer time-scales ($t \approx$ 300 ps), some water molecules have traveled as far as 3 Å. In the range of 300 ps to 3 ns, mobile water molecules accumulate at the first hopping site characterized by the increase of intensity over the time of $G_s(r,t)$ at 3 Å, length of a water molecule (Figure 4(a)). The average jump length in C–S–H ($\approx$3 Å) is more than three times larger than that of bulk water at room temperature ($\approx$0.9 Å).[68] The average jump length in supercooled water at 253 K is roughly 2.4 Å[69] which is close to that computed for C–S–H. This is another reason that suggests water in the interlayer space behaves like supercooled liquids. The hopping mechanism to the farther sites occurs at longer time-scales.

The first water molecules arrive at the second hopping site after 3 ns. At longer time-scales, up to 6 ns, it can be concluded from the vanishing of the first peak that the probability of the presence of water molecules in the cage decreases, the second and third peaks grow signaling dominant diffusive mode. This probabilistic picture is reminiscent of picosecond local structural fluctuations within dynamical basin and slow inter-basin jumps as seen in supercooled liquids.[70] This brings about the notion of "lower effective temperature" suggested

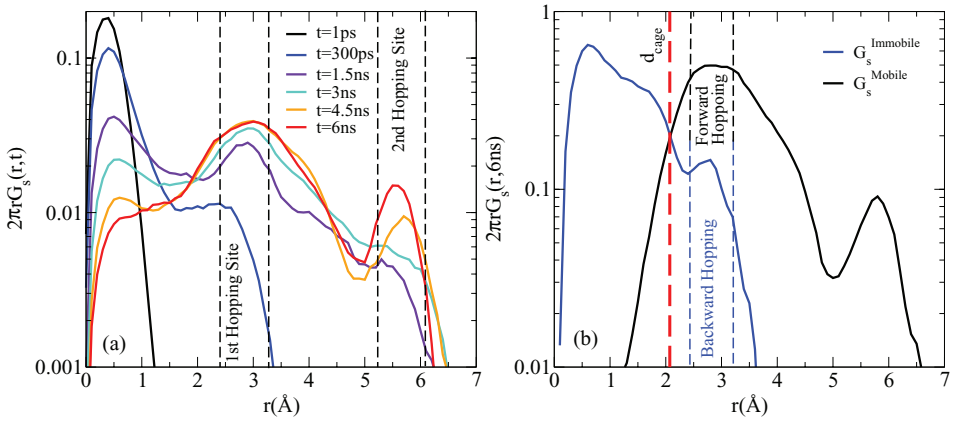

FIG. 4. Description of the collective diffusion of water molecules using Van Hove space-time correlation function. (a) Van Hove correlation function of water molecules in a C–S–H sample with Ca/Si = 1.4 at different time steps. (b) The Van Hove correlation function at 6 ns plotted for mobile and immobile water molecules.

by both neutron diffraction experiments[71] and molecular dynamics simulations of water in hydrophilic surfaces.[23] Specifically, Gallo *et al.*[23] observed that water molecules adjacent to hydrophilic surfaces behave as they do below their mode coupling crossover temperature in pores as large as 4 nm even when modeled at ambient conditions. However, this homogenous description of water diffusion only explains the diffusive motion of mobile water molecules.

The heterogeneity in the dynamics of water molecules in the interlayer spacing of C–S–H is very similar to heterogeneous dynamics of ionic[72] and supercooled liquids[73] in which particles diffuse with significantly different residence times at different regions only a few angstroms apart. To distinguish between the water molecules with different residence times, the self part of Van Hove function is decomposed into mobile, $G_s^M(r,t)$, and immobile, $G_s^I(r,t)$, components:

$$G_s^M(r,t) = \frac{1}{N_M}\sum_{i=1}^{N_M}\langle\delta(r-|r_i(t+\tau)-r_i(\tau)|)\rangle, \quad (5)$$

$$G_s^I(r,t) = \frac{1}{N_I}\sum_{i=1}^{N_I}\langle\delta(r-|r_i(t+\tau)-r_i(\tau)|)\rangle, \quad (6)$$

where N_M and N_I are the number of mobile and immobile water molecules, respectively. The distinction between mobile and immobile species is made based on their individual MSDs. If the average displacement is less than the cage size, $\mathrm{RMSD}_i < \mathrm{d}_{cage}$, then the water molecule is considered as immobile. Otherwise, it is categorized as mobile. Figure 4(b) presents the mobile-immobile decomposition of the Van Hove function. For time-scales up to 6 ns, the immobile water librating within the cage might overpass the cage size and briefly spend time in the first hopping zone. This is explained by the presence of the minor peak in $\mathrm{G}_s^{Immobile}$ at r = 3 Å in Figure 4(b). It should be emphasized that, since the MSDs of immobile water molecules are less than 2 Å, any transgression beyond cage size is temporary. This is a clear sign of the backward hopping mechanism in which water oscillates between the cage and the first hopping site. On the other hand, some of mobile water molecules might briefly spend some time at the boundary of the cage. However, these molecules elapse most of their time in the first and second hopping sites. Some of the water molecules oscillate back and forth which is characterized by the forward and backward hopping mechanism from first to second hopping sites. This forward and backward hopping is also experimentally observed in the diffusion of hydrogen on TiO_2 surfaces in which forward hopping is favored depending on separation distance.[74] The enhancement of interstitial molecules in the first coordination shell constraints large displacements. Therefore, diffusion of water molecules necessitates highly correlated displacements of many water molecules referred to as cooperative hopping mechanism.[75] This cooperative hopping mechanism increases the probability of backward hopping as collective diffusion in confined environment attributes to higher diffusion energy barriers. Such collective mobility depends strongly on the chemistry of adsorption surface; as further explained in Sec. III D.

D. Composition-dependent water mobility

The heterogeneity in confined water dynamics is systematically analyzed by studying mobility across samples of varying composition. Figure 5 shows the Van Hove function at 6 ns for five C–S–H samples with Ca/Si ratios varying from 1.1 to 1.8. At very low Ca/Si ratios distinguished by crystalline substrate close to that of tobermorite minerals, Ca/Si = 1.12, all of the water molecules are confined within their cage. In this case, the whole Van Hove function is limited within the cage radius, d_{cage}. In Figure 6, the motion of water molecules is depicted by superposing the positions of water molecules at different time steps starting at 1 fs up to 6 ns, covering six orders of magnitude in the time domain. As depicted in the first row of Figure 6, at low Ca/Si ratios, the motion of water molecules is restricted to libration adjacent to their adsorption sites (interlayer calcium atoms and defective silica chains). At this stoichiometry, the motion of water molecules is described as "pocket-like" behavior which emphasizes their localized motion. This localized behavior is related to abundance of bridging SiO_2 groups protruding into the interlayer spacing which effectively obstructs the

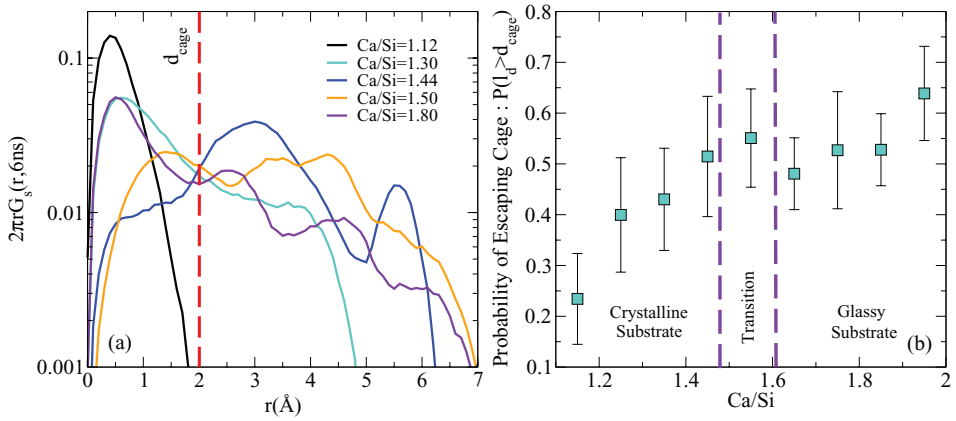

FIG. 5. The effect of composition on the mobility of water molecules in the C–S–H interlamellar spacing. (a) Van Hove correlation function at t = 6 ns plotted for C–S–Hs of varying composition. (b) Probability of water molecules to escape the cage as a function of the Ca/Si ratio.

diffusive motion of water molecules in the channel. At a slightly higher Ca/Si ratio, Ca/Si = 1.30, more bridging groups are removed from the silicate chains. This provides the opportunity for some water molecules to escape their cage and enter their first hopping site. At the transition regime, most of the bridging sites are removed from the silica chains, which fully open the diffusion channel. As described before, a significant portion of water molecules opens to the first and second hopping sites. As highlighted in the second row of Figure 6, the water molecules oscillate within the cage up to 10 ps and start to diffuse at longer residence times in the order of 100 ps. For those substrate compositions, we define the diffusive motion of water molecules as being "patch-like" diffusion. As presented in the third row of Figure 6

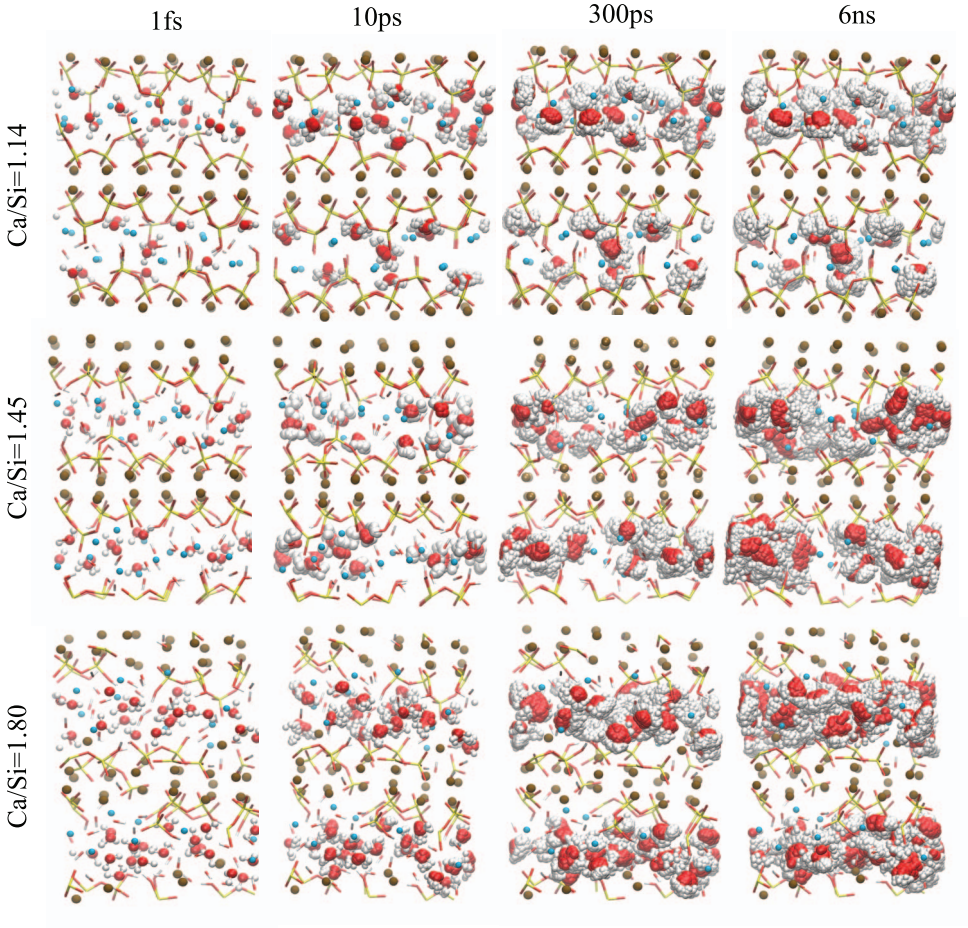

FIG. 6. Visualization of the space that water molecules explore within the C–S–H interlayer for three different samples with Ca/Si ratios equal to 1.14 (crystalline substrate), 1.45 (transition substrate), and 1.80 (glassy substrate). The water molecules are superposed at 10 ps, 300 ps, and 6 ns at the intervals of every 1 ps. The brown and cyan spheres represent intralayer and interlayer calcium ions, respectively. Red and yellow sticks depict silicate tetrahedra. White-red sticks represent hydroxyl groups and white and red sticks with white and red spheres display water molecules.

(Ca/Si = 1.8), the diffusive channels are fully developed making individual trajectories hard to distinguish. We define this as an "in-channel" diffusion. In order to quantify the impact of substrate compositions on the mobility of water molecules, we calculate the probability of a water molecule escaping the cage after 6 ns, P(d > d_{cage}), which we define as

$$P(d > d_{cage}) = \frac{1}{A_n} \int_{d_{cage}}^{\infty} 2\pi r G_s(r, t = 6\,\text{ns}) dr, \quad (7)$$

where d is displacement and A_n denotes the normalizing factor defined as $\int_0^{\infty} 2\pi r G_s(r, t = 6\,\text{ns}) dr$. This escaping probability increases linearly with Ca/Si ratio within the crystalline C–S–H regime. Then it reaches to a plateau, which is mainly due to the absence of bridging sites in the interlayer. However, at large Ca/Si ratios, the mobility increases due to the fact that immobile water molecules provide screening against the coulombic interactions between the calcium-silicate substrate and mobile water molecules. Because of the aforementioned screening effect, which was pointed out as the origin of the plateau in the dipole moment of water molecules as well (see Figure 2(a)), the dipole moment and mobility are strongly correlated. In addition both follow a bilinear trend with Ca/Si ratio.

E. Self-diffusion of ultraconfined water in C–S–H interlayer

As discussed above, the diffusion of water molecules inside the C–S–H particles is inhomogeneous and anisotropic. This as well as the quasi two-dimensional nature of collective diffusive motion of mobile water molecules, defines the self-diffusivity of water for planar component of the mobile water species. Following the Einstein relation in 2D:

$$D_{\parallel} = \frac{1}{4} \lim_{t \to \infty} \frac{MSD_{xy}(t)}{t}. \quad (8)$$

It is made sure that the diffusion regime is achieved in the simulations and the uncertainty in measuring long time limit is considered in error bars reporting self-diffusivity values. In addition to this uncertainty, the description of water diffusion by $D_{\parallel}$ entails an approximation. However, the ratio of $D_{\perp}/D_{\parallel}$ is quite negligible for especially mobile water molecules. The effect of substrate composition on the self-diffusivity of water molecules is presented in Figure 7. The self-diffusivity of water in the interlayer, $D_{C\text{–}S\text{–}H}$, is normalized by that of bulk SPC water at 300 K, D_{H_2O}, 4.17 × 10^{-9} m^2s^{-2}. Analogous to the probability of escaping cage, $D_{C\text{–}S\text{–}H}$ increases linearly in the crystalline domain and maintains a constant value at the glassy regimes. Due to the high H_2O/Si ratio at very high Ca/Si ratios, the self-diffusivity increases further because of the abovementioned screening effect. $D_{C\text{–}S\text{–}H}$ in high Ca/Si ratio, 0.0018 × D_{H_2O}, is almost three times higher than that of low Ca/Si ratio, 0.0006 × D_{H_2O}. This highlights the effect of substrate composition on the diffusion of water molecules in the ultraconfined hydrophilic environments. On average, the self-diffusivity of water in the interlayer spacing inside C–S–H particles is thousand times slower than that of bulk water. This emphasizes that part of the mobile interlayer water diffuses with significantly slow dynamics, however distinguishable from the dynamics of immobile water and hydroxyl groups. Bordallo *et al.*[76] briefly mentioned this existence of a dynamics slower than that of glassy water and attributed it to proton exchange in the interlayer. Based on the present description of water mobility in C–S–H, this dynamics can be related to diffusion of mobile water in the interlayer. It is noteworthy that water in tobermorite minerals (Ca/Si > 1) is immobile as it does not have translational motion at the scale of 10 ns (water molecules experience librating motion). This means that tobermorite minerals cannot provide insightful

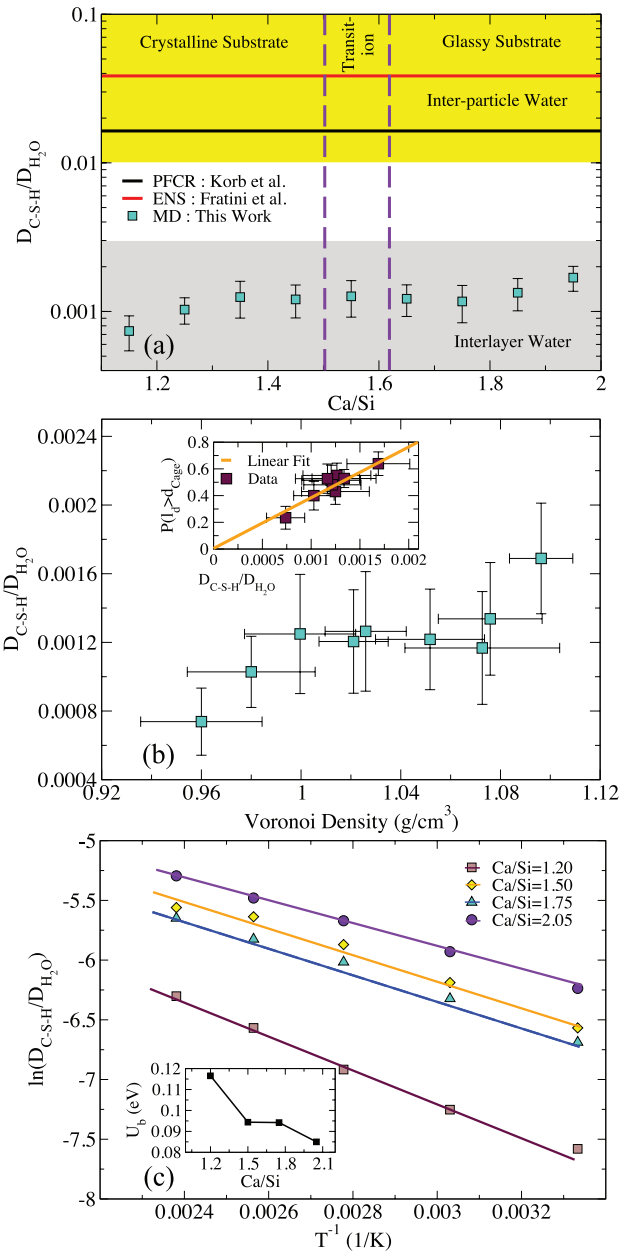

FIG. 7. Mobility of water in C–S–H's interlayer spacing. (a) Effect of C–S–H composition on the self-diffusivity of interlayer water compared against Elastic Neutron Scattering (ENS) and Proton Field Cycling Relaxometry technique (PFCR). (b) Anomalous correlation between density and self-diffusivity of confined water in C–S–H. The inset provides the relation between the self-diffusivity and probability of escaping the cage. (c) Scaling of self-diffusivity with inverse temperature for four C–S–H models with different Ca/Si ratio. The inset presents the diffusion energy barrier as a function of Ca/Si ratio.

information for studying water in C–S–H with common composition of Ca/Si = 1.7. In C–S–H, the diffusion of mobile interlayer water is different from inter-particle water molecules and those on the surface of larger pores.

The values of self-diffusivities presented in this study are at least one order of magnitude less than that measured by PFCR by Korb *et al.*[77] (D_{H_2O}/80) and Incoherent Elastic Neutron Scattering measurements of Fratini *et al.*[19] (D_{H_2O}/60). Recent ENS experiments suggest that slow self-diffusion in the paste is associated with inter-particle water.[78] PFCR experiments are interpreted to capture the dynamical behavior of water adsorbed on the pore surfaces.[20] In particular, Kalinichev *et al.*[79] reported MD simulation of adsorbed water on [100] surfaces of anomalous tobermorite with self-diffusions comparable to that of Korb *et al.*[20] Since the inter-particle pore-size distribution is shown to be significantly larger than interlayer spacing,[80] the significant difference in characteristic length of confinement explains the difference between the self-diffusion inside and in between C–S–H grains. Recently, Coasne *et al.*[81] have critically reviewed the state of the art of water in mesoporous systems shedding light on the dynamics in mesopores in between C–S–H particles. The contrast between the intra- and inter-particle water is also observed in hydrated bundles of imogolite nanotubes.[82]

Studying properties of bulk water has led to identification of several unusual behaviors known as anomalous features of water.[83,84] Prielmeier *et al.*[85] discovered an anomaly in which self-diffusivity of bulk water increases with pressure with a maximum at 200 MPa. Scala *et al.*[86] showed that for supercooled water at 220 K, the self-diffusivity of bulk water increases with density with a maximum at 1.15 g/cm^3. This anomalous behavior was also shown to exist for SiO_2 glassy structure[87] and magmatic liquids.[88] Figure 7(b) presents the correlation between the density and self-diffusivity of water in the interlayer voids of C–S–H. Having many features in common with supercooled liquids, the self-diffusivity of water in the interlayer of C–S–H increases with the density. However, these anomalies have different sources in supercooled liquids and ultraconfined water in between hydrophilic surfaces. In supercooled water, the collapse of hydrogen bond network under external pressure is believed to increase the diffusivity of water.[89] In contrast, the physical reason behind the peculiar behavior in C–S–H is related to the increase in probability of escaping cage. As described in the inset of Figure 7(b), the correlation between the probability of escaping cage for water molecules that have been identified as mobile, $P(d > d_{cage})$, and their relative self-diffusion, $D_{C\text{-}S\text{-}H}/D_{H_2O}$ is linear ($P(d > d_{cage}) = 400 \times D_{C\text{-}S\text{-}H}/D_{H_2O}$). The diffusion energy barrier is equal to the kinetic energy required for a water molecule to break its surrounding cage and diffuse. It can be estimated via the Arrhenius relation,

$$D_{C-S-H} = D_{H2O} \times \exp\left(\frac{-U_b}{k_B T}\right), \tag{9}$$

where U_b, k_B, and T are diffusion energy barrier, Boltzmann constant, and temperature, respectively. In molecular dynamics, U_b can be estimated by gradually increasing the temperature of the system and monitoring the logarithm of self-diffusivity as a function of the inverse temperature. To measure U_b in C–S–H models of varying composition, five simulations were performed in the range of 300 K to 420 K for four C–S–H models with Ca/Si ratios equal to 1.2, 1.5, 1.75, and 2.05 (Fig. 7(c)). It is important to note that $ln\,(D_{C\text{-}S\text{-}H})$ scales linearly with the inverse temperature which means that Arrhenius relation is still valid in these describing diffusion in nano-confined environments. The slope of these lines is proportional to U_b which are plotted in the inset of Fig. 7(c). The energy barrier is in the order of 0.12 eV at low Ca/Si ratios (Ca/Si = 1.2) and decreases to 0.08 eV at high Ca/Si ratio (Ca/Si = 2.05). This explains the abovementioned anomalous behavior in the self-diffusivity of nano-confined water in which despite the increase in density, the diffusion energy barrier decreases. The reduction in the energy barrier is at the origin of the increase in the self-diffusivity and the probability of escaping the cage with increasing Ca/Si ratio. We note that this decrease of energy barrier is fully similar to what was observed for supercooled sodium silicate liquids.[90] Again, this supports the idea that water in C–S–H shows a supercooled-type dynamics.

IV. CONCLUSION

The properties of confined water in the interlayer spacing of C–S–H, a class of defective porous calcium-silicates, were carefully studied using the molecular dynamics method over a set of 150 samples with Ca/Si ratio ranging from 1.1 to 2.1. The C–S–H substrate compositions (hence nanotexture) directly affects the structural properties of ultraconfined water such as bond length, dipolar moment, density, or average number of hydrogen bonds. It is found that the dipole moment, Voronoi density, and the number of hydrogen bonds per water molecules increase with the Ca/Si ratio. The water dynamics in the interlayer spacing was characterized as quasi two-dimensional in which the diffusion in the direction of layers is the dominant mode. The mean square displacement shows a four stage dynamics reminiscent of those in supercooled liquids and glassy phases. In addition, both MSD and Van Hove space-time correlation function indicated significant heterogeneity in the water dynamics. The mean hopping distance was found to be around 2.8 Å, roughly the size of a water molecule, the size comparable to that observed in supercooled water. The decomposition of Van Hove function into mobile and immobile contributions provides a new perspective of the dynamics of immobile water molecules. In addition, it reveals the possibility of backward hopping from the first hopping site to the center of the so-called dynamical cage.

More importantly, however, the mobility of water is found to be strongly composition-dependent. It increases with increasing Ca/Si ratios by up to one order of magnitude. Over the whole range of Ca/Si ratio, the diffusivity of mobile water is 1/1000th of the bulk water. The increase in the probability of escaping the dynamical cage with increasing Ca/Si ratio physically explains the composition-dependent mobility in relation to the amount of protruding silica groups in the interlayer spacing of C–S–H. This brings forward the notion of "pocket-like," "patch-like," and "in-channel" diffusion at low, medium, and high Ca/Si ratios, respectively. Strong interaction with the C–S–H hydrophilic surfaces and their

sub-nanometric defective texture reduces the self-diffusivity of mobile water molecules. Furthermore, self-diffusivity of water in the interlayer is roughly ten times smaller than the one observed in elastic neutron scattering and proton field-cycling relaxometry experiments, which only probe the dynamics of water in C–S–H's meso-pores. Hence, these experiments are not yet addressing the water dynamics inside the nanotexture of C–S–H. Finally, there is a correlation between the structural and dynamical properties in terms of correlation between density and self-diffusivity. Similar to the anomalous behavior of bulk water, the self-diffusivity of water in the nanotexture of C–S–H increases with the density. The confined water in C–S–H is shown to have higher self-diffusivity due to increase in the escaping probability from the dynamical cage through reduction of diffusion energy barriers. Overall, this work paves the way to further understand the properties of confined water in hydrophilic ultra-confining disordered porous materials.

ACKNOWLEDGMENTS

The concrete Sustainability Hub at MIT has supported this work with sponsorship provided by the Portland Cement Association (PCA) and the NRMCA Research and Education Foundation. With great pleasure, M.J.A.Q. acknowledges many fruitful discussions with Dr. Benoit Coasne, Dr. Jeff Thomas, Dr. Davoud Ebrahimi, and Professor Hamlin Jennings.

[1] M. Elimelech and W. A. Phillip, Science **333**, 712–717 (2011).
[2] M. Sanlés-Sobrido, M. Pérez-Lorenzo, B. Rodríguez-González, V. Salgueiriño, and M. A. Correa-Duarte, Angew. Chem. Int. Ed. **51**, 3877–3882 (2012).
[3] F. Nouar, J. Eckert, J. F. Eubank, P. Forster, and M. Eddaoudi, J. Am. Chem. Soc. **131**, 2864–2870 (2009).
[4] T. Roussel, C. Bichara, K. E. Gubbins, and R. J. M. Pellenq, J. Chem. Phys. **130**, 174717 (2009).
[5] H. Furukawa and O. M. Yaghi, J. Am. Chem. Soc. **131**, 8875–8883 (2009).
[6] Y. Chen, H. Chen, D. Zeng, Y. Tian, F. Chen, J. Feng, and J. Shi, ACS Nano **4**, 6001–6013 (2010).
[7] M. Chaplin, Nat. Rev. Mol. Cell Biol. **7**, 861–866 (2006).
[8] A. Fernández and M. Lynch, Nature (London) **474**, 502–505 (2011).
[9] K. Shirono and H. Daiguji, Chem. Phys. Lett. **417**, 251–255 (2006).
[10] A. Eftekhari-Bafrooei and E. Borguet, J. Am. Chem. Soc. **132**, 3756–3761 (2010).
[11] G. Cicero, J. C. Grossman, E. Schwegler, F. Gygi, and G. Galli, J. Am. Chem. Soc. **130**, 1871–1878 (2008).
[12] M. Vandamme, F.-J. Ulm, and P. Fonollosa, Cem. Concr. Res. **40**, 14–26 (2010).
[13] R. J.-M. Pellenq, N. Lequeux, and H. van Damme, Cem. Concr. Res. **38**, 159–174 (2008).
[14] L. B. Skinner, S. R. Chae, C. J. Benmore, H. R. Wenk, and P. J. M. Monteiro, Phys. Rev. Lett. **104**, 195502 (2010).
[15] A. J. Allen, J. J. Thomas, and H. M. Jennings, Nat. Mater. **6**, 311–316 (2007).
[16] G. Constantinides and F.-J. Ulm, J. Mech. Phys. Solids **55**, 64–90 (2007).
[17] W.-S. Chiang, E. Fratini, P. Baglioni, D. Liu, and S.-H. Chen, J. Phys. Chem. C **116**, 5055–5061 (2012).
[18] E. Masoero, E. Del Gado, R. J.-M. Pellenq, F.-J. Ulm, and S. Yip, Phys. Rev. Lett. **109**, 155503 (2012).
[19] E. Fratini, A. Faraone, F. Ridi, S.-H. Chen, and P. Baglioni, J. Phys. Chem. C **117**, 7358–7364 (2013).
[20] J.-P. Korb, P. McDonald, L. Monteilhet, A. Kalinichev, and R. Kirkpatrick, Cem. Concr. Res. **37**, 348–350 (2007).
[21] J. J. Thomas, S. A. FitzGerald, D. A. Neumann, and R. A. Livingston, J. Am. Ceram. Soc. **84**, 1811–1816 (2001).
[22] M. Youssef, R. J.-M. Pellenq, and B. Yildiz, J. Am. Chem. Soc. **133**, 2499–2510 (2011).
[23] P. Gallo, M. Rovere, and E. Spohr, Phys. Rev. Lett. **85**, 4317–4320 (2000).
[24] E. Fratini, S.-H. Chen, P. Baglioni, and M.-C. Bellissent-Funel, Phys. Rev. E **64**, 020201 (2001).
[25] E. Fratini, S.-H. Chen, P. Baglioni, and M.-C. Bellissent-Funel, J. Phys. Chem. B **106**, 158–166 (2002).
[26] H. Manzano, S. Moeini, F. Marinelli, A. C. T. van Duin, F.-J. Ulm, and R. J.-M. Pellenq, J. Am. Chem. Soc. **134**, 2208–2215 (2012).
[27] X. Cong and R. Kirkpatrick, Adv. Cem. Based Mater. **3**, 144–156 (1996).
[28] R. J.-M. Pellenq, A. Kushima, R. Shahsavari, K. J. V. Vliet, M. J. Buehler, S. Yip, and F.-J. Ulm, Proc. Natl. Acad. Sci. U.S.A. **106**, 16102–16107 (2009).
[29] S. Hamid, Z. Kristallogr. **154**, 189–198 (1981).
[30] M. J. Abdolhosseini Qomi, F.-J. Ulm, and R. J.-M. Pellenq, J. Am. Ceram. Soc. **95**, 1128–1137 (2012).
[31] M. J. Abdolhosseini Qomi, M. Bauchy, R. J.-M. Pellenq, and F.-J. Ulm, in *Mechanics and Physics of Creep, Shrinkage, and Durability of Concrete: A Tribute to Zdenk P. Bazant*, edited by M. J. AbdolhosseiniQomi, M. Bauchy, R. J.-M. Pellenq, and F.-J. Ulm (American Society of Civil Engineers, 2013), pp. 78–85.
[32] P. J. van Maaren and D. van der Spoel, J. Phys. Chem. B **105**, 2618–2626 (2001).
[33] K. Smirnov and D. Bougeard, Chem. Phys. **292**, 53–70 (2003).
[34] O. Teleman, B. Jonsson, and S. Engstrom, Mol. Phys. **60**, 193–203 (1987).
[35] F. Sedlmeier, D. Horinek, and R. R. Netz, J. Am. Chem. Soc. **133**, 1391–1398 (2011).
[36] R. Shahsavari, R. J.-M. Pellenq, and F.-J. Ulm, Phys. Chem. Chem. Phys. **13**, 1002–1011 (2011).
[37] R. T. Cygan, J.-J. Liang, and A. G. Kalinichev, J. Phys. Chem. B **108**, 1255–1266 (2004).
[38] D. Wolf, P. Keblinski, S. R. Phillpot, and J. Eggebrecht, J. Chem. Phys. **110**, 8254–8282 (1999).
[39] See supplementary material at http://dx.doi.org/10.1063/1.4864118 for details on the preparation of C–S–H structures and the force fields.
[40] S. Plimpton, J. Comput. Phys. **117**, 1–19 (1995).
[41] S. V. Churakov, Am. Mineral. **94**, 156–165 (2009).
[42] P. A. Bonnaud, B. Coasne, and R. J.-M. Pellenq, J. Phys. Condens. Matter **22**, 284110 (2010).
[43] J. Puibasset and R. J.-M. Pellenq, J. Phys. Chem. B **112**, 6390–6397 (2008).
[44] R. Kumar, J. R. Schmidt, and J. L. Skinner, J. Chem. Phys. **126**, 204107 (2007).
[45] B. Auer, R. Kumar, J. R. Schmidt, and J. L. Skinner, Proc. Natl. Acad. Sci. U. S. A. **104**, 14215–14220 (2007).
[46] A. D. Hammerich and V. Buch, J. Chem. Phys. **128**, 111101 (2008).
[47] A. Luzar and D. Chandler, Phys. Rev. Lett. **76**, 928–931 (1996).
[48] A. Luzar and D. Chandler, Nature (London) **379**, 55–57 (1996).
[49] J. L. Dashnau, N. V. Nucci, K. A. Sharp, and J. M. Vanderkooi, J. Phys. Chem. B **110**, 13670–13677 (2006).
[50] D. Ebrahimi, R. J.-M. Pellenq, and A. J. Whittle, Langmuir **28**, 16855–16863 (2012).
[51] P. Yu, R. J. Kirkpatrick, B. Poe, P. F. McMillan, and X. Cong, J. Am. Ceram. Soc. **82**, 742–748 (1999).
[52] J. J. Thomas, H. M. Jennings, and A. J. Allen, J. Phys. Chem. C **114**, 7594–7601 (2010).
[53] F. W. Starr, S. Sastry, J. F. Douglas, and S. C. Glotzer, Phys. Rev. Lett. **89**, 125501 (2002).
[54] I.-F. W. Kuo and C. J. Mundy, Science **303**, 658–660 (2004).
[55] M. Matsumoto, S. Saito, and I. Ohmine, Nature (London) **416**, 409–413 (2002).
[56] B. Halle and M. Davidovic, Proc. Natl. Acad. Sci. U.S.A. **100**, 12135–12140 (2003).
[57] A. Kuffel and J. Zielkiewicz, J. Phys. Chem. B **116**, 12113–12124 (2012).
[58] M. G. Mazza, N. Giovambattista, F. W. Starr, and H. E. Stanley, Phys. Rev. Lett. **96**, 057803 (2006).
[59] M. C. Pitman and A. C. T. van Duin, J. Am. Chem. Soc. **134**, 3042–3053 (2012).
[60] W. Kob, J. Phys. Condens. Matter **11**, R85 (1999).
[61] A. Roder, W. Kob, and K. Binder, J. Chem. Phys. **114**, 7602–7614 (2001).
[62] D. Caprion, J. Matsui, and H. R. Schober, Phys. Rev. Lett. **85**, 4293–4296 (2000).

[63]D. Argyris, D. R. Cole, and A. Striolo, J. Phys. Chem. C **113**, 19591–19600 (2009).
[64]S. Romero-Vargas Castrillón, N. Giovambattista, I. A. Aksay, and P. G. Debenedetti, J. Phys. Chem. B **113**, 7973 (2009).
[65]T. G. Lombardo, N. Giovambattista, and P. G. Debenedetti, Faraday Discuss. **141**, 359 (2009).
[66]P. Chaudhuri, L. Berthier, and W. Kob, Phys. Rev. Lett. **99**, 060604 (2007).
[67]M. Bauchy and M. Micoulaut, Phys. Rev. B **83**, 184118 (2011).
[68]J. Teixeira, M.-C. Bellissent-Funel, S. H. Chen, and A. J. Dianoux, Phys. Rev. A **31**, 1913–1917 (1985).
[69]S.-H. Chen, P. Gallo, and M.-C. Bellissent-Funel, Can. J. Phys. **73**, 703–709 (1995).
[70]J. Qvist, H. Schober, and B. Halle, J. Chem. Phys. **134**, 144508–144508 (2011).
[71]H. Li, W.-S. Chiang, E. Fratini, F. Ridi, F. Bausi, P. Baglioni, M. Tyagi, and S.-H. Chen, J. Phys. Condens. Matter **24**, 064108 (2012).
[72]Z. Hu and C. J. Margulis, Proc. Natl. Acad. Sci. U.S.A. **103**, 831–836 (2006).
[73]M. D. Ediger, Annu. Rev. Phys. Chem. **51**, 99–128 (2000).
[74]S.-C. Li, Z. Zhang, D. Sheppard, B. D. Kay, J. M. White, Y. Du, I. Lyubinetsky, G. Henkelman, and Z. Dohnalek, J. Am. Chem. Soc. **130**, 9080–9088 (2008).
[75]R. Zangi and S. A. Rice, Phys. Rev. E **68**, 061508 (2003).
[76]H. N. Bordallo, L. P. Aldridge, and A. Desmedt, J. Phys. Chem. B **110**, 17966–17976 (2006).
[77]J.-P. Korb, L. Monteilhet, P. McDonald, and J. Mitchell, Cem. Concr. Res. **37**, 295–302 (2007).
[78]H. Li, E. Fratini, W.-S. Chiang, P. Baglioni, E. Mamontov, and S.-H. Chen, Phys. Rev. E **86**, 061505 (2012).
[79]A. G. Kalinichev, J. Wang, and R. J. Kirkpatrick, Cem. Concr. Res. **37**, 337–347 (2007).
[80]P. McDonald, V. Rodin, and A. Valori, Cem. Concr. Res. **40**, 1656–1663 (2010).
[81]B. Coasne, A. Galarneau, R. J. M. Pellenq, and F. D. Renzo, Chem. Soc. Rev. **42**, 4141–4171 (2013).
[82]B. Creton, D. Bougeard, K. S. Smirnov, J. Guilment, and O. Poncelet, Phys. Chem. Chem. Phys. **10**, 4879 (2008).
[83]R. Ludwig, Angew. Chem. Int. Ed. **40**, 1808–1827 (2001).
[84]L. Xu, P. Kumar, S. V. Buldyrev, S.-H. Chen, P. H. Poole, F. Sciortino, and H. E. Stanley, Proc. Natl. Acad. Sci. U.S.A. **102**, 16558 (2005).
[85]F. X. Prielmeier, E. W. Lang, R. J. Speedy, and H.-D. Ludemann, Ber. Bunsenges. Phys. Chem. **92**, 1111–1117 (1988).
[86]A. Scala, F. W. Starr, E. La Nave, F. Sciortino, and H. E. Stanley, Nature (London) **406**, 166–169 (2000).
[87]J. R. Errington and P. G. Debenedetti, Nature (London) **409**, 318–321 (2001).
[88]M. Bauchy, B. Guillot, M. Micoulaut, and N. Sator, Chem. Geol. **346**, 47 (2013).
[89]P. G. Debenedetti and F. H. Stillinger, Nature (London) **410**, 259–267 (2001).
[90]M. Bauchy and M. Micoulaut, Phys. Rev. Lett. **110**, 095501 (2013).